Answer to Referee 1

We wish to thank to this referee for his/her very useful comments, which have helped us to improve the manuscript, and have been addressed as follows:

General comments:

1. *The paper presents an algorithm for the integration of air parcel trajectories in three dimensions and the computation of the function M for the analysis of Lagrangian transport, and it is applied to atmospheric reanalyzed data for the study of the Antarctic stratospheric vortex. The paper is clearly written, and visualization of the Lagrangian geometry of the stratospheric vortex shows potential. However, the paper lacks of new scientific results. While I cannot recommend publication, I encourage the authors to address my concerns below and resubmit.*

We have clarified in the new version of the article the major goal, as maybe this was not sufficiently clear in the original manuscript. In the new version we state very clearly that the goal is to describe 3D Lagrangian structures on the stratosphere. To this end we have described in more detail (Section 2) what kind of 3D Lagrangian structures are expected in the stratosphere and we list specifically what are the new scientific results in this regard in the Abstract, Section 5 and the Conclusions.

2. *Regarding the first part, the authors state in the abstract "The present paper introduces an algorithm for the visualization, analysis and verification of transport and mixing processes in three-dimensional atmospheric flows". While sections 2 and 3 present the methodology in a very clear and concise way, I do not a find significant novelty in this part of the paper.*

• *Neither the reanalysis data processing, nor the parcel trajectory methods are new (the way they handle the singularity at the poles in geographical coordinates seems identical to that published by some of the co-authors in De la Camara et al. 2012).*

• *The authors have published multiple articles analyzing transport in oceanic and atmospheric flows using the function M to highlight the Lagrangian geometry of such flows. The extension to 3D, while interesting, does not constitute a new advance from a methodological point of view since the authors have already introduced it in at least a couple of studies (Mancho et al. 2013, Lopesino et al. 2017). Besides, the function M is conceptually defined for n-dimensional fields (Mancho et al. 2013).*

The referee is right. The algorithm is not new, and that sentence has been modified. The previous applications of the function M to 3D flows are summarised between lines 19 and 25 in the Introduction. Regarding the algorithm, what is new is its implementation for analysing 3D atmospheric data sets as stated in line 36 of the Introduction. We mantain the section describing the implementation of the algorithm (Section 3) because it may be useful to other researchers interested in applying this tool for similar purposes.

3. *I do not quite understand the verification part of the study. Section 4.1 visually compares maps of the function M obtained from 2D isentropic calculations and from full 3D calculations (Fig 1). But, if I am not mistaken, the authors use the same set of equations (5) for both the 2D and 3D calculations; the only difference is that in 2D the*

vertical velocity w is zero. Does this mean the authors verify their 3D integration code against itself?

The 2D calculation is done on constant potential temperature surfaces which in general are surfaces which are time dependent and do not coincide with spherical shells. The velocity fields on these surfaces are also downloaded from ERA-interim. The 3D calculation is done in the 3D space with 3D velocity fields downloaded from ERA-interim and processed as explained in the article. Section 4 now discusses these issues and has been extended to include calculations showing cases in which the 3D calculation on spherical shells and the 2D calculation on the constant potential temperature surfaces coincide (upper stratosphere) and where they do not (upper troposphere).

4. *Figure 2 does a much better job at verifying the function M code by comparing maps of M with geopotential height and potential vorticity (PV) fields. Sadly, the authors do not discuss this figure at all (see lines 16-20). Why is the anticyclone that we see in the height field not visible in the PV or M fields? What are the expected differences between PV and M? What about the tongue of high PV (red colors) wrapping around the vortex? Why is there no equivalent structure in the M map?*

Also, it is rather confusing to analyze maps of these three diagnostics, each using different vertical coordinates. I recommend the authors to interpolate the data to a common horizontal surface.

Figure 2 (now figure 3) has been thoroughly explained in Section 4. The issues rised by the referee have been addressed including a new figure.

The different vertical coordinates used for each map are standard in atmospheric sciences and we are plotting for each one the value which is in correspondence to their partners. We do not think that differences in the units is a problem.

5. *It is argued throughout the paper that stratospheric motions are basically isentropic for timescales of 10 days. While I understand the authors choice of an integration time of 5 days in Fig. 1 to compare against isentropic trajectories, why using again tau = 5 days in section 4.2 to analyze the 3D Lagrangian geometry of the vortex? Are the results not practically identical to 2D isentropic calculations if the trajectories are integrated over time periods when the isentropic assumption is valid? A way of checking this point would be to perform isentropic calculations at different vertical levels in the stratosphere, and plot similar figures 3-8 (longitude versus height).*

We have compared isentropic calculations and 3D calculations in the new Figures 2 and 3 in Section 4 and it is shown when they coincide or not. We also discuss the effect of the integration period τ on M. Additionally we have explained more clearly what new insights are brought by our results. Indeed, the 3D calculations allow to perform slices in directions perpendicular to plane of motion and those sections highlight the structure of normally hyperbolic invariant objects whose vertical structure cannot be visualized otherwise. To our knowledge such visualisation is described for the first time in this article.

6. • *I strongly encourage the authors to increase tau to explore the full potential of 3D calculations. Is there a value of tau over which the Lagrangian geometry from 2D (isentropic) and 3D significantly and 3D diverge?*

We have done this in Section 4.

7. *Besides, one problem of using the wind field in geometrical height coordinates is that it is difficult to assess what part of the vertical motion is due to the vertical displacement of isentropic surfaces. To prove the added value of the 3D calculations, I recommend using the velocity field in potential temperature surfaces (the vertical velocity would therefore be the heating rate, see Diallo et al 2012 ACP).*

The wind field in geometrical coordinates is useful to integrate equations (7). The integration of this system has allowed us to describe 3D Lagrangian structures in the stratosphere. In particular we describe to our knowledge for the first time the following issues: vertical extension of the stratospheric polar vortex and its lower limit and its tilted character. We have identified the boundary between troposphere and stratosphere. We have identified lagrangian structures, fully 3D, showing strong mixing into the troposphere. We have discussed the vertical structures of two counterrotating vortices, (the polar vortex and a new emerging one) and identified an invariant structure separating them and have related this to the presence of a normally hyperbolic invariant curve. For all this purposes our approach has shown to be sufficient and consistent with other results, thus we do not think it is necessary to repeat calculations within another approach. To address the issues regarding transport across potential temperature surfaces is a very interesting question feasible also within our approach (just calculating M on the time dependent potential temperature surfaces) but out of the scope of the current manuscript.

8. *2) I do not see any new insights into the dynamics or transport of the polar vortex.*

• *The description of the evolution of the stratospheric flow during the spring season is, as the authors acknowledge, basically the same as that given in much earlier studies. What have we learned from the analysis of the function M? Is this description richer from that offered by dynamically relevant fields such as geopotential height or PV? I am afraid not*

We have explained in the current version very clearly what are the novel insights on the stratosphere provided by our work. It might be that our discussions in the first version were too much focused in addressing consistency with previous findings, and our findings were not sufficiently emphasized. For this reason we have rewritten the manuscript to address these issues. A list of specific new insights are described in the 7th bullet point, and further discussion about the comparison with the geopotential height and PV is given in the new version.

9. *One needs a very trained eye to see the geometrical structures that the authors highlight in Figs. 7 and 8 (hyperbolic trajectories and invariant manifolds). How are these structures identified? How is its hyperbolic nature assigned? Also, those structures seem to be located in the outer side of the westerly jet, just in the region where Joseph and Legras (2002 JAS), with similar tools, described a region of chaotic motions. I think this paper does not offer new significant insights into the nature of this region. The fact that the authors identify vertical transport barriers (hardly seen by untrained eyes) does not mean that the motions responsible for those structures are three-dimensional. Again, a detailed comparison between 3D and isentropic calculations is needed.*

We have introduced a new Section 2 which introduces and mathematically describes the type of 3D Lagrangian structures expected in the stratosphere. A relevant example is introduced. We have added extra arrows in current figures 8 and 9 to highlight the

geometrical structures we are interested in and those are linked with the example described in the new Section 2.

Figure 9 a) is similar to the projections performed by Josep and Legras, although in that article they do not discuss the event we address in this figure about the boundary separating two counterrotating vortices present in the atmosphere. The advantage of the used tools with respect to the FSLE used by Joseph and Legras is that the M function highlights simultaneously manifolds and coherent structures related to elliptic regions.

On the other hand figures showing the vertical structure across the stratosphere are new and to our knowledge have not been described before.

Figure 8 address the invariant character of structures related to sharp changes in the color code of M. This is done by tracking a particle trajectory and observing that during its evolution, its position stays on a line with an abrupt change in the M color code.

A detailed comparison between 3D and isentropic calculations is addressed now in figures 3 and 4.

Answer to Referee 2

We wish to thank to this referee for his/her very useful comments, which have helped us to improve the manuscript, and have been addressed as follows:

Issues:

1. *The claim is that structures are identified in a 3D flow. But I would expect to see some extracted 2D structures, as was done in the cited paper du Toit, P. C. and Marsden, J. E. (2010). However, this is not the case. We merely see cross-sections of what are presumably 2D structures in the 3D flow.*

The Introduction of the new version of the manuscript explains (from lines 8 to 28) different approaches used to identify 3D Lagrangian structures in 3D flows. The one by du Toit and Marsden is one but not the only one. In the new Section 2 these issues raised by the referee are carefully addressed. Our approach consist of the use of function M and this methodology gains insights in the 3D flow by computing the function M on slices with different orientation. This approach does not compute surfaces representing the 2D invariant manifolds, but obtains them by means of slices and has the advantage of highlighting tori-like structures.

2. *How to identify elliptical LCS from the M function should be stated more clearly.*

We have done this in Section 2.

3. *The use of the term algorithm in this paper is a bit confusing. Usually one expects to see a set of step by step instructions or a flow chart associated with an algorithm.*

We have done this in Section 3.2.

Insights on the three-dimensional Lagrangian geometry of the Antarctic Polar Vortex

Jezabel Curbelo[1,2], Víctor ~~J.~~ José García-Garrido[1], Carlos ~~R.~~ Roberto Mechoso[3], Ana ~~M.~~ Maria Mancho[1], Stephen Wiggins[4], and Coumba Niang[1,5]

[1]Instituto de Ciencias Matemáticas, CSIC-UAM-UC3M-UCM. C/ Nicolás Cabrera 15, Campus de Cantoblanco UAM, 28049 Madrid, Spain.
[2]Departamento de Matemáticas, Facultad de Ciencias, Universidad Autonóma de Madrid, 28049 Madrid, Spain.
[3]Department of Atmospheric and Oceanic Sciences, University of California at Los Angeles, Los Angeles, California.
[4]School of Mathematics, University of Bristol. Bristol BS8 1TW, UK.
[5]Laboratoire de Physique de l'Atmosphere et de l'Ocean Simeon Fongang, Ecole Superieure Polytechnique, Universite Cheikh Anta Diop, 5085, Dakar-Fann, Senegal.

Abstract. ~~The present paper introduces an algorithm for the visualization, analysis and verification of transport and mixing processes in~~ In this paper we study the three-dimensional ~~atmospheric flows. This algorithm is based on the methodology of Lagrangian descriptors (LDs) , a technique from Dynamical Systems Theory. The algorithm is applied to reanalysis data in~~ (3D) Lagrangian structures in the Stratospheric Polar Vortex (SPV) above Antarctica. We analyse and visualize these structures using the Lagrangian descriptor function M. The procedure for calculation with reanalysis data is explained. Benchmarks are computed and analysed that allow us to compare 2D and 3D aspects of Lagrangian transport. Dynamical systems concepts appropriate to 3D, such as normally hyperbolic invariant curves, are developed and applied. In order to illustrate ~~the evolution of~~ our approach we select an interval of time in which the SPV is relatively undisturbed (August 1979) and an interval of rapid SPV changes (October 1979). Our results provide new insights on the Lagrangian structure of the vertical extension of the ~~flow above Antarctica during a period of rapid changes in the southern spring of 1979. The evolution of Lagrangian coherent structures is discussed and connections with the stratosphere is examined. The results suggest that the cyclonic~~ stratospheric polar vortex ~~during late winter appears to extend down to the troposphere. The results are also indicative of features related to invariant manifolds that can act as deep vertical barriers to transport between vortices~~and its evolution. Our results also show complex Lagrangian patterns indicative of strong mixing processes in the upper troposphere and lower stratosphere. Finally, during the transition to summer in the late spring, we illustrate the vertical structure of two counterrotating vortices, one the polar and the other an emerging one, and the invariant separatrix that divides them.

1 Introduction

Over the past several decades the mathematical theory of dynamical systems has provided a fruitful framework to describe the transport and mixing proceses that take place in fluids and to understand the underlying flow structures associated with these phenomena. The seminal paper by Aref (1984) on chaotic advection sparked interest in this perspective, which is inspired by the work of Poincaré. For the understanding of particle dynamics, Poincaré sought a geometrical approach that was based on

geometrical structures and their role in organizing all trajectories into regions corresponding to qualitatively different dynamical fates. These structures have been referred to as Lagrangian Coherent Structures (LCS) in the fluid mechanics community (Haller and Yuan, 2000; Shadden *et al.*, 2005).

Many studies of LCS in the atmosphere and in the ocean have been performed in a two-dimensional (2D) scenario. This is because in an appropriate range of space and time scales a Lagrangian property of the particles is approximately unchanged in time. Hence, the flow can be assumed to occur on surfaces on which that property is constant. For instance, stratospheric flows in the time scale of stratospheric sudden warmings ($\sim$10 days) are, to a first approximation, adiabatic and frictionless, and thus fluid particles and their trajectories are constrained to remain on surfaces of constant specific potential temperature (isentropic surfaces). Bowman (1993) and ~~?~~ Joseph and Legras (2002) have examined transport processes across the Antarctic stratospheric polar vortex (SPV) on isentropic surfaces, which are quasi-horizontal in the atmosphere. Also, for oceanic flows it is often assumed that fluid parcels remain on surfaces of constant density (isopycnals), which are quasi-horizontal. Mancho *et al.* (2006b); d'Ovidio *et al.* (2009); Branicki *et al.* (2011) followed the isopycnal approach for oceanic applications in the Mediterranean Sea, Mendoza *et al.* (2014) for the Gulf of Mexico and Garcia-Garrido *et al.* (2015, 2016) for other ocean areas.

Geophysical flows, however, are not 2D. The study of transport processes in 3D flows brings into the discussion issues about the three-dimensional (3D) visualization of Lagrangian structures (see e.g. Wiggins (2010)). In idealized 3D time-dependent flows Poincaré sections have been used to recognize significant Lagrangian structures (Cartwright *et al.*, 1996; Pouransari *et al.*, 2010; Moharana *et al.*, 2013; Rypina *et al.*, 2015). Invariant manifolds acting as transport barriers in 3D flows may have the structure of convoluted 2D surfaces embedded in a volume (Branicki and Wiggins, 2009). In oceanic contexts these surfaces have been identified by stitching together 2D Lagrangian structures at different layers (Branicki and Kirwan Jr., 2010) or connecting ridges computed from Finite Size Lyapunov exponent fields (Bettencourt *et al.*, 2014). In the field of atmospheric sciences, these structures have similarly been obtained by connecting ridges computed from Finite Time Lyapunov Exponents (FTLE) (Rutherford and Dangelmayr, 2010; du Toit and Marsden, 2010; Lekien and Ross, 2010). More recently, also in atmospheric contexts, 3D Lagrangian information has been extracted by means of 2D slices of the full 3D FTLE field computed from 3D trajectories (Rutherford *et al.*, 2012).

The ~~present paper introduces an algorithm for the visualization, analysis and validation of transport and mixing processes in~~ methodology used in this paper for visualizing 3D ~~atmospheric flows. The methodology~~ Lagrangian structures in the stratosphere is based on the Lagrangian descriptor known as the function M (Madrid and Mancho, 2009; Mendoza and Mancho, 2010; Mancho *et al.*, 2013)~~, computed in 3D~~. So far, ~~the~~ in the stratosphere context, the function M has been used ~~in 2D settings~~ to gain insight into key dynamical and transport processes in ~~the stratosphere~~ 2D settings (de la Cámara *et al.*, 2012, 2013; Smith and McDonald, 2014; Guha *et al.*, 2016; Manney and Lawrence, 2016; García-Garrido *et al.*, 2017). More recently, (Mancho *et al.*, 2013; Lopesino *et al.*, 2017) have applied the function M to the visualization of structures in idealized 3D flows. Rempel *et al.* (2013) have applied the function M to visualize coherent structures in full 3D direct numerical simulations of the compressible magnetohydrodynamic equations. The function M has the advantage of highlighting simultaneously invariant manifolds by means of singular features and also tori-like coherent structures (see ~~Mendoza and Mancho (2010); de la Cámara *et al.* (2012); Rempel *et al.* (2013); Lopesino *et al.* (2017)~~Mendoza and Mancho (2010); de la

In here we apply M to produce a full 3D description from 3D flows above Antarctica during a period in the spring of 1979 ~~when there were rapid changes in the stratosphere~~ in which the stratosphere was both rather stable (August) and subjected to rapid changes (October) (Yamazaki and Mechoso, 1985). In this region, the later period selected for analysis comprises an interval when the winter circulation, which is characterized by a strong circumpolar westerly (cyclonic) flow known as the Stratospheric Polar Vortex (SPV), breaks down as the final warming to summer condition develops. Although final warmings in the southern hemisphere are broadly similar each year (Mechoso *et al.*, 1988b), can be punctuated by periods of rapid changes. During the final warming of 1979, the transition from the winter to the summer circulation accelerated during mid-October, a period when perturbing waves were very active and the vertical energy flux from the troposphere intensified (Yamazaki and Mechoso, 1985). Our aim is to describe and visualize these phenomena from a full 3D perspective using reanalysis data. To our knowledge, this is the first time that the potential of M to achieve this goal is explored.

The article is organized as follows. Section 2 describes the ~~dataset used for the study of the Antarctic final warming of 1979 and the post-processing needed for the Lagrangian analysis~~dynamical systems approach to the analysis of 3D Lagrangian structures. Section 3 describes the dataset used in this study, the calculation of M in 3D~~and details the~~ , the data post-processing needed to this end, the computational procedures and other issues involved in this task. Section 4 discusses some benchmark calculations and their interpretation. Section 5 provides the results and findings of M on the 3D Lagrangian structure of the polar vortex on August and mid-October 1979. Finally, section ~~5~~ 6 includes a discussion and presents our conclusions.

2 The Dynamical Systems Approach to the Analysis of 3D Lagrangian Structures

3 ~~Dataset and Post-processing~~

2.1 ~~ERA-Interim Reanalysis Data~~

The theory of dynamical systems provides an ideal framework for studying nonlinear transport and mixing processes in the atmosphere. The geometrical structures that vertebrate the Lagrangian skeleton act as material barriers that fluid particles cannot cross. A key element on the dynamical description are the presence of hyperbolic regions defined by rapid fluid contracting and expanding rates along directions that are respectively associated to the stable and unstable manifolds. In 2D flows, these manifolds are curves while in 3D settings other possibilities arise. We discuss some particularities for the system under study next.

If we assume that air parcels are passively advected by the flow, the dynamical system that governs the atmospheric flow is given by:

$$\dot{\mathbf{x}} = \mathbf{v}\left(\mathbf{x}\left(t\right), t\right) \;\; , \;\; \mathbf{x}\left(t_0\right) = \mathbf{x}_0 \; , \tag{1}$$

where $\mathbf{x}\left(t; \mathbf{x}_0\right)$ represents the trajectory of an air parcel that at time t_0 is at position $\mathbf{x}_0$, and $\mathbf{v}$ is the velocity field. For the geophysical context we are focusing on, the velocity components will be supplied by the ERA-Interim reanalysis dataset produced at the European Centre for Medium-Range Weather Forecast as explained in detail in the next section. As it will be

verified in there, the magnitude of the vertical velocity component in the middle and upper stratosphere is very small so that vertical displacements of fluid parcels compared to the horizontal displacements are also small for the time scales of interest in this study (∼days). These considerations motivate the discussion of a system with the particular structure given in Eq. (2) as it will support the interpretation of the findings described in Section 5 in this region of the atmosphere.

For two dimensional flows hyperbolic trajectories and their stable and unstable manifolds are the key kinematical features responsible for the geometrical template governing transport. However, in three dimensions there are new types of three dimensional structures that may form a geometrical template that governs transport. The ''weak three dimensionality" of many geophysical flows, like the one considered in this paper, gives rise to a (normally) hyperbolic invariant curve (i.e. not a single trajectory) that has two dimensional stable and unstable manifolds embedded in the 3D space. In this case the stable and unstable manifolds of this invariant curve are codimension one in the flow and therefore provide barriers to transport. Moreover, since in this case the stable and unstable manifolds are both codimension one they can intersect to form lobes, resulting in a three dimensional version of lobe dynamics. We now describe the special form of the flow giving rise to this structure. The form of the flow follows from Wiggins (1988) and was described in the context of fluid mechanics in Mezić and Wiggins (1994).

Here we examine a simple model three dimensional velocity field that captures the form of the velocity field given by the data set that we study and, therefore, allows us to describe this less familiar notion of a normally hyperbolic invariant curve in a simple setting. The velocity field has the following form:

$$\begin{cases} \dfrac{dx}{dt} = \dfrac{\partial H(x,y,z,t)}{\partial y} = v_x(x,y,z,t) \\ \dfrac{dy}{dt} = -\dfrac{\partial H(x,y,z,t)}{\partial x} = v_y(x,y,z,t) \\ \dfrac{dz}{dt} = 0 \end{cases} , \tag{2}$$

where $H(x,y,x,t) = A(z)\sin(\pi y)\sin(\pi x)/\pi$ and $A(z) = 1+\sin(\pi z/2)$. The system is defined in the domain $(x,y,z) \in [0,1]\times[-1,1]\times$ We refer to x and y as the horizontal coordinates and z as the vertical coordinate. This velocity field is certainly ''weakly" three dimensional as there is no motion in the vertical direction yet the horizontal motion does depend on the height. This model contains the essence of the geometrical structures governing transport in the data set that we analyze.

More specifically, note that for each z the system (2) has a hyperbolic fixed point at $(x=0, y=0)$, for which the linearized system is:

$$\frac{dx}{dt} \approx A(z)\pi x, \tag{3}$$

$$\frac{dy}{dt} \approx -A(z)\pi y. \tag{4}$$

The curve $(0,0,z)$ is clearly an invariant curve (in particular, it is a curve of fixed points). The linearized stability described by (4) quantifies linearized stability *normal* to the invariant curve $(0,0,z)$ and, hence, is the origin of the phrase *normal hyperbolicity*. For each z, the fixed point has a one dimensional stable manifold and a one dimensional unstable manifold.

Therefore as a function of z the curve $(0, 0, z)$ has two dimensional stable and two dimensional unstable manifolds in three dimensions. Hence, these two dimensional invariant surfaces provide barriers to transport in the three dimensional flow (Wiggins, 1988; Mezić and Wiggins, 1994). The geometrical representation of the manifolds is shown in Figure 1a).

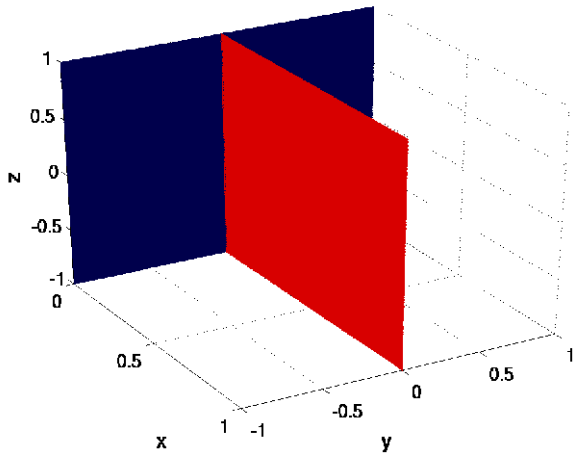

a)

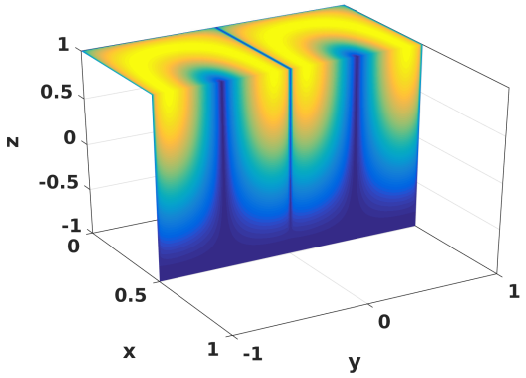

b)

Figure 1. a) Stable (blue) and unstable (red) manifolds of the normally hyperbolic invariant curve in Eq. (2); b) representation of the Lagrangian structures at specific slices by means of the function M.

The 3D Lagrangian structure of Eq. (2) visualised in Figure 1b), is achieved by means of the function M, which is represented on slices intersecting the manifolds. Other slice choices are possible, but here we just show two simple possibilities on perpendicular planes which help to capture the essential features of the full 3D motion. The function M is defined as follows:

$$M(\mathbf{x}_0, t_0, \tau) = \int_{t_0-\tau}^{t_0+\tau} \|\mathbf{v}(\mathbf{x}(t; \mathbf{x}_0), t)\| \, dt \, , \tag{5}$$

where $\mathbf{v}(\mathbf{x},t)$ is the velocity field and $\|\cdot\|$ denotes the Euclidean norm. At a given time t_0, M corresponds to the length of the trajectory traced by a fluid parcel starting at $\mathbf{x}_0 = \mathbf{x}(t_0)$ as it evolves forwards and backwards in time for a time interval τ. For sufficiently large τ values the sharp changes that occur in narrow gaps in the scalar field provided by M, which we will refer to as singular features, highlight the stable and unstable manifolds and, at their crossings, hyperbolic trajectories as confirmed by Figure 1b). Recently, Lopesino *et al.* (2017) have established a rigorous mathematical foundation for specific LDs for a class of examples in continuous time dynamical systems.

Figure 1b) shows that the function M has also the capability of revealing vortices present in the fluid. In particular for this example two counterrotating vortices which are vertically extended are visible. The yellowish colours highlight the part of vortices with highest speeds. Typically vortex or jet like structures (for periodic domains) are related to 2-tori in three dimensional flows. This is discussed in Mezić and Wiggins (1994); Wiggins (2010). This notion is related to fluid regions trapping fluid parcels in their interior and isolating them from the surrounding fluid as for instance is the case of the circulating strong jet forming the SPV. There exist formal results linking contourlines of the time average of M with tori-like invariant sets. In this manner singular lines in 1b) highlight invariant manifolds and contourlines of converged averages of M highlight invariant tori (see Lopesino *et al.* (2017)).

3 Dataset and computation of the function M

3.1 ERA-Interim Reanalysis dataset

We use the ERA-Interim Reanalysis dataset produced by European Centre for Medium-Range Weather Forecasts (ECMWF;Simmons *et al.* (2007)). The usefulness of this dataset for the Lagrangian study of atmospheric flows from the dynamical systems perspective is ~~assured~~ established by the results of several previous studies. For instance, de la Cámara *et al.* (2013) applied Lagrangian Descriptors (LDs) to study the structure of the ~~southern polar vortex during the 2005 southern spring and compared the LCS obtained with~~ SPV during the southern spring of 2005, to support the interpretation of several features found in the trajectories of superpressure balloons released from Antarctica by the VORCORE project (Rabier *et al.*, 2010). ERA-Interim covers the period from 1979 to the present day (Dee *et al.*, 2011)~~and it~~ , and can be downloaded from http://apps.ecmwf.int/datasets/data/interim-full-daily/levtype=sfc/.

From the ERA-Interim dataset we ~~use the~~ extract the 3D wind velocity components, potential vorticity, surface pressure~~and also~~ , and the geopotential field. ~~These~~ In the version of the dataset that we selected for the present study, these physical variables are available four times daily (00:00 06:00 12:00 18:00 UTC) with a horizontal resolution of $0.75^\circ \times 0.75^\circ$ in longitude and latitude. ~~We take the velocity fields at the sigma~~ The velocity fields extracted correspond to the 60 hybrid-sigma levels of the model component of the reanalysis system (~~60 levels in the vertical from 1000 to~~ from the Earth's surface to the 0.1 hPa ~~). Moreover, we take~~ level) . We also take from the dataset potential vorticity at 15 levels of potential temperature (265, 275, 285, 300, 315, 330, 350, 370, 395, 430, 475, 530, 600, 700, 850; K), and geopotential ~~field at hPa~~ at field pressure levels (1, 2,

3, 5, 7, 10, 20, 30, 50, 70, 100 to 250 by 25, 300 to 750 by 50, 775 to 1000 by 25~~). For the calculation of parcel trajectories, as needed to compute~~ ; hPa).

3.2 Computation of the function M

The procedure to obtain the function M ~~, the wind fields are transformed from sigma to geometric height(80 levels that range from 0 m to 47600 m with a step of 600 m) .~~

3.3 ~~Data post-processing~~

~~Our goal is to compute particle trajectories on spatial coordinates , and for this reason we need to transform the wind fields from the model levels (used in the ERA-Interim Reanalysis) to height (in meters). For the post-processing of the dataset we use the Climate Data Operator (CDO) software (available at https://code.zmaw.de/projects/cdo). The input provided to the CDO~~ in (lat, lon, height) coordinates from the data described in the previous section consists of the ~~three velocity components in sigma levels, and of surface pressure, which is available every six hours on a global grid of $0.75° \times 0.75°$.~~ following steps.

Step 1. The data is downloaded from ERA-Interim in `.grib` format and on a monthly basis~~and is stored daily in separate files in order to avoid handling very large data files when computing particle trajectories that require interpolation~~.

~~To transform the data from hybrid sigma (model) levels to height using CDO, first one concatenates each wind component with the surface pressure using the CDO command mergeand later one needs to convert the data files~~ Step 2. The data files are converted from `.grib` to `.nc` format. This is done with the command `copy`, setting as arguments `-t ecmwf` to indicate that the data is from ERA-Interim and `-f nc` to specify that the output complies with NetCDF. ~~Next, we apply the CDO~~

Step 3. The 3D velocity and 2D surface pressure data are concatenated to provide the input to the Climate Data Operator (CDO) software (available at https://code.zmaw.de/projects/cdo) using the CDO command ~~`ml2hlxmerge`~~ ~~to the NetCDF files, which converts data at the sigma levels of ERA-Interim~~ .

Step 4. The data is converted from sigma levels to the height levels ~~that we select for our analysisand extrapolate the missing data . The vertical spatial interpolationis performed over~~ specified for the analysis, and required data are produced by interpolation, with the vertical velocity expressed in ms^{-1}. This is done using the CDO command `ml2hlx` applied to the NetCDF files. The resulting 3D velocity field has a horizontal resolution of $0.75° \times 0.75°$ in longitude and latitude, with 80 height levels ~~that range~~ ranging from 0 m to 47600 m ~~with a step of~~ at 600 m intervals. Each wind data variable is stored in separate files by day ~~;~~ using the commands `selvar` and `selday`~~are used for this process.~~ . This procedure avoids the handling very large data files when computing particle trajectories, which requires interpolation in time and space.

4 ~~The Dynamical Systems Approach to the Analysis of Lagrangian Structures~~

~~The theory of dynamical systems provides an ideal framework for studying nonlinear transport and mixing processes in the atmosphere. The geometrical structures that vertebrate the Lagrangian skeleton act as material barriers that fluid particles cannot cross. A key element on the dynamical description is the distinction between hyperbolic and elliptic regions. Hyperbolic~~

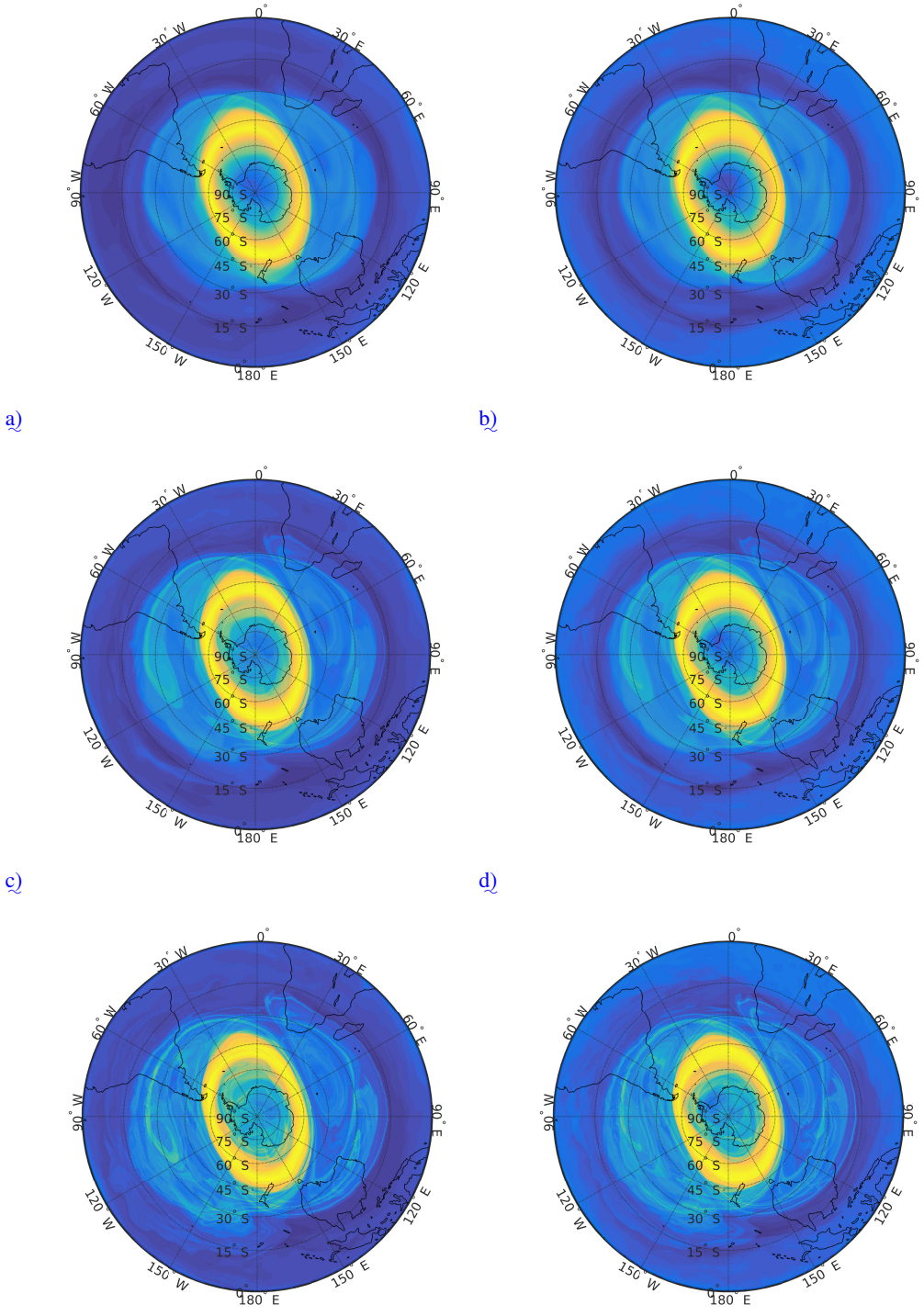

Figure 2. M calculated on the 15th August at 1979 00:00:00 UTC: a) using a 2D approach where particle trajectories are constrained to the 850K potential temperature level and $\tau = 5$ days; b) M computation for $\tau = 5$ days using a full 3D computation of trajectories and it is represented at a constant height level of $h = 31.3$ km (which corresponds approximately to the 850K isentropic surface); c) the same as a) with $\tau = 10$ days ; d) the same as b) with $\tau = 20$ days ; e) the same as a) with $\tau = 20$ days.

regions are defined by rapid fluid contracting and expanding rates along directions that are respectively associated to the stable and unstable manifolds. In 2D flows, these manifolds are curves while in 3D settings other possibilities arise in which manifolds are complex and convoluted 2D surfaces embedded in the 3D space. This makes the array of possible spatial configurations richer and their visualization much more complex. A discussion on the notion of elliptic regions is given for instance in (Mancho *et al.*, 2013). Heuristically for us in this article, this notion is related to fluid regions trapping fluid parcels in their interior and isolating them from the surrounding fluid as for instance is the case of the circulating strong jet forming the SPV.

The diagnostic that we will use to build the Lagrangian skeleton of the atmosphere is the function M, which is defined in the following way:

$$M(\mathbf{x}_0, t_0, \tau) = \int_{t_0-\tau}^{t_0+\tau} \|\mathbf{v}(\mathbf{x}(t;\mathbf{x}_0),t)\|\, dt\,,$$

where $\mathbf{v}(\mathbf{x},t)$ is the velocity field and $\|\cdot\|$ denotes the Euclidean norm. At a given time t_0Step 5. To avoid issues at the pole in the calculation of trajectories from equations expressed in spherical coordinates, we write the velocities in cartesian coordinates from the velocity data available in spherical coordinates (see de la Cámara *et al.* (2012)); The velocity components in cartesian coordinates are given by, M corresponds to the length of the trajectory traced by a fluid parcel starting at $\mathbf{x}_0 = \mathbf{x}(t_0)$ as it evolves forwards and backwards in time for a time interval τ. As τ increases a richer Lagrangian history is incorporated into M, and a more complex and detailed dynamical description is obtained. The sharp changes that occur in narrow gaps in the scalar field provided by M, which we will refer to as singular features, highlight the stable and unstable manifolds and, at their crossings, hyperbolic trajectories (see for example Fig. 2). This tool has also the capability of revealing the vortices present in the fluid. Recently, Lopesino *et al.* (2017) have established a rigorous mathematical foundation (at specific examples) for specific LDs in continuous time dynamical systems.

If we assume that air parcels are passively advected by the flow, the dynamical system that governs the atmospheric flow is given by:

$$\dot{\mathbf{x}} = \mathbf{v}\left(\mathbf{x}\left(t\right),t\right) \;\;,\;\; \mathbf{x}\left(t_0\right) = \mathbf{x}_0\,,$$

where $\mathbf{x}\left(t;\mathbf{x}_0\right)$ represents the trajectory of an air parcel that at time t_0 is at position $\mathbf{x}_0$, and $\mathbf{v}$ is th velocity field.

$$\begin{cases} v_x = w\cos\lambda\cos\phi - u\sin\lambda - v\cos\lambda\sin\phi, \\ v_y = w\sin\lambda\cos\phi + u\cos\lambda - v\sin\lambda\sin\phi, \\ v_z = w\sin\phi + v\cos\phi, \end{cases} \quad . \tag{6}$$

The computation of M requires the integration of particle trajectories by means of numerically integrating (1). In geographic coordinates Eq. (1) can be written as:

$$\begin{cases} \dfrac{d\lambda}{dt} = \dfrac{u(\lambda,\phi,h,t)}{(R+h)\cos\phi} \\ \dfrac{d\phi}{dt} = \dfrac{v(\lambda,\phi,h,t)}{R+h} \\ \dfrac{dh}{dt} = w(\lambda,\phi,h,t) \end{cases} ,$$

where u, v, and w are the zonal, meridional, and vertical velocity components, respectively, λ is longitude, and ϕ is latitude~~, h is elevation (height) above the Earth's surface and $R = 6371$ km is the mean Earth radius. Observe that in these spherical coordinates there is a singularity at the poles. To avoid this issue, we will calculate trajectories using a~~ .

Step 6. The trajectories are calculated in a cartesian coordinate system, ~~the equations for the trajectories in this system are:~~

$$\begin{cases} \dfrac{dx}{dt} = v_x(\lambda,\phi,h,t) \\ \dfrac{dy}{dt} = v_y(\lambda,\phi,h,t) \\ \dfrac{dz}{dt} = v_z(\lambda,\phi,h,t) \end{cases} ,$$

~~in which the velocity components are given by :~~ which are obtained by solving,

$$. \begin{cases} \dfrac{dx}{dt} = v_x(\lambda,\phi,h,t) \\ \dfrac{dy}{dt} = v_y(\lambda,\phi,h,t) \\ \dfrac{dz}{dt} = v_z(\lambda,\phi,h,t) \end{cases} , \tag{7}$$

To integrate the system (7) the data interpolation of the fields v_x, v_y, v_z is carried out by interpolating u, v, w in spherical coordinates, since the post-processed data files from ERA-Interim are expressed in this way. In order to do so, we have used the `griddedInterpolant` function provided by the MATLAB© software, which generates an object that can be saved into memory and evaluated at any point of interest in the trajectory at a later time. This allows ~~us~~ for substantial saving in computational time at every integration step. Moreover, when applying this function to interpolate the dataset, we specify that a cubic interpolation is used in space and also in time. The ~~dynamical~~ system (7) is integrated using a Cash-Karp Runge-Kutta scheme (Press *et al.*, 1992) with a time step of 1 hour~~and we impose the boundary condition of $w = 0$ for the vertical velocity of air particles at the Earth's surface (i. e. ~~ . The condition $w = 0$ is imposed at $h = 0$ ~~).~~ in order to constrain trajectories in the vertical. Important computational savings are also achieved by integrating simultaneously the whole meshgrid of initial conditions by using a matrix formulation. Additionally, the computational time is reduced by running the MATLAB© software with options requiring the use of multiple cores.

h	
31.3 km	
10 days remain, to a first approximation, on surfaces of constant specific potential temperature (isentropic surfaces) which are themselves quasi-horizon	

Table 1. Comparison of the values taken by velocity components at different atmospheric levels.

4 Results

Step 7. The function M is obtained by approximating the integral in (5) by the sum of the lengths (in the euclidean space) of the segments linking the position of the integrated particle trajectory at two successive time steps. As τ increases a richer Lagrangian history is incorporated into M, and a more complex and detailed dynamical description is obtained.

3.1 Benchmark simulations

We note that for the ERA interim data set w is very small in the upper stratosphere at 31.3 km (see Table 1 for values during the period September-October 1979). Moreover, the mean value of w at that level is 100 times less than the maximum value, with a very low mean dispersion. Table 1 also shows that in the upper troposphere levels at 10 km) the values of w are comparatively not as small.

As indicated earlier, the trajectories of fluid particles in stratospheric flows at time scale of $\sim$

4 Benchmarks

To benchmark the procedure described in the previous sections is to section, we compare the Lagrangian outputs obtained from the full 3D scenario at a constant height constant heights (spherical shells) with those obtained from the 2D scenario for a potential temperature surface that is at approximately potential temperature surfaces that are approximately at the same height. Figure 2a) shows As expected from results in table 1, given that $w \sim 0$ in the upper stratosphere, the potential temperature surface and the spherical shell are expected to be almost identical. Figure 2 compares for different τ values, the evaluation of the function M with $\tau = 5$ days for a 2D integration in the 850K isentropic surface . The with that obtained on a spherical shell at 31.3 km height, which approximately corresponds to the 850K surface. For $\tau = 5, 10$ days the figure highlights well defined structures (de la Cámara *et al.*, 2012) that are very similar in both cases. These consist of a large circulating coherent vortex in yellow, representing high values of M that are related to particles exhibiting large displacements and blueish zones corresponding to calmer regions. Lobes eroding the outer part of the vortex are clearly identified by colored filaments. Also crossings of contours of M highlighting hyperbolic trajectories are noticed along longitudes 15^{o}W and 165 ^{o}E. The height

~~level that corresponds to the 850K surface is approximately 31.3km. Figure 2b) shows the output of M at this constant height for a full~~

Increasing the τ values to 20 or 30 days adds more Lagrangian detail to the figures, which thus contain long term transport issues reflected in very thin and long filamenteous structures. However the figures at constant potential temperature and constant height are still very similar and contain the gross structure already observed at smaller τ. Differences are restricted to those filamenteous structures which are difficult to follow and to compare. Given that long term transport issues are difficult to interpretate and that we do not require them for describing the phenomena of our interest which occur in time intervals varying from hours to 10 days, we fix in this range the selected τ values for this article.

Comparisons of transport between both approaches in the upper troposphere are rather different, as figure 3 confirms. In this case table 1 shows significant non zero vertical velocities, and thus surfaces of constant potential vorticity are expected not to be close to simple spherical shells. The first row shows the 2D calculations for a 2D integration in the 330K isentropic surface for a period of $\tau = 5, 10$ days and the second row a 3D ~~integration with $\tau = 5$. A very similar pattern is found, which supports the correctness of the results reflecting the small departures of fluid particles from the quasi-horizontal isentropic surface in the time scale of a few days.~~ output at the corresponding height (10km) for the same integration intervals. Clear differences are observed in the images that are visible even at the shorter integration period of $\tau = 5$ days. This confirms that in this case the potential temperature surface is not close to the spherical shell for which the 3D calculations are shown. Results discussed in the next section will show further evidence of the 2D-3D motions transitions.

~~Figure 4 shows further comparisons at different days in October 1979.~~

Figure 4 contrasts the more classical description of events in the middle-upper stratosphere with the one provided by our Lagrangian descriptor. The left hand column of Figure 4 shows the geopotential height at 10mb. This field is ~~related with~~ particularly useful because it is equivalent to the velocity streamfunction at the corresponding presure level in the extratropics (see García-Garrido *et al.* (2017)). This field provides a purely Eulerian description of the flow, however in the time dependent case this point of view is limited as it does not address issues regarding the fate of particle trajectories. The middle column shows the picture provided by the potential vorticity at the 850K equivalent temperature (isentropic) surface. ~~In the~~ This field is conserved along particle trajectories, thus the image is Lagrangian in the sense that we observe the field of a purely advected quantity. The right hand column ~~we show outputs obtained from~~ shows the function M at the surface $z = 31.3$ km obtained from particle trajectories in full 3D calculations~~of the function~~ . Similarly to the second column the displayed information is Lagrangian, but here we obtain more fundamental information in this regard. This figure provides feedback for characterising the time evolution of any purely advected scalar field, while the previous one displays just the realisation of one particular initial data. More specifically, the third column highlights the position and evolution of two hyperbolic points in the outer part of the vortex, as well as the vortex itself. As discussed by García-Garrido *et al.* (2017) hyperbolic points are responsible for filamentation processes. Whether or not these filaments are eventually observed depends on the distribution of the scalar field. For instance if the scalar field is completely uniform in the whole domain then its time evolution will show nothing about the features highlighted by M~~at the surface $z = 31.3$km. These results are further demonstration of the consistency of our algorithm.~~

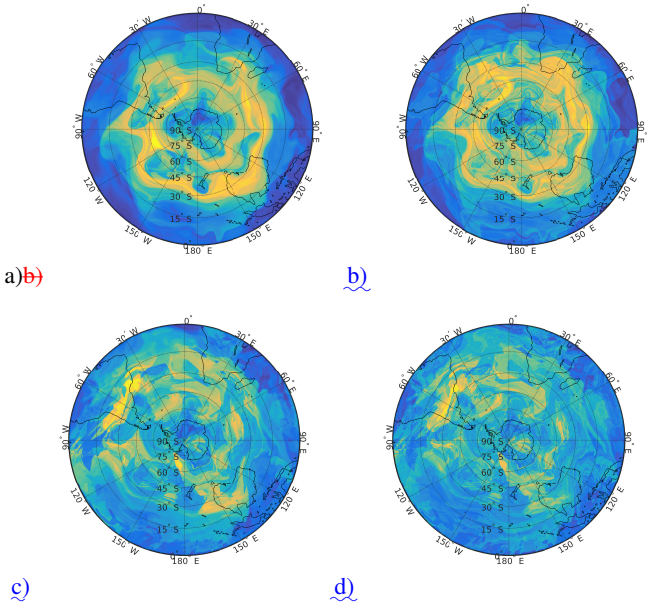

Figure 3. M calculated on the 15th August at 1979 00:00:00 UTC~~with $\tau = 5$~~: a) using a 2D approach where particle trajectories are constrained to the ~~850K~~ 330K potential temperature level and $\tau = 5$ days; b) the same with $\tau = 10$ days; c) M calculated for $\tau = 5$ days using a 3D computation of trajectories and represented at a constant height level of ~~$h = 31.3$~~ $h = 10$ km (which corresponds approximately to the ~~850K~~ 330K isentropic surface); d) the same with $\tau = 10$ days.

~~Geopotential Potential vorticity~~ . How the features of the M ~~function~~ field are visible in a scalar field depends on how is the initial distribution of the advected field, with respect to the features of M. Figure 5 illustrates these facts in a very simple example. Figure 5 a) highlights the Lagrangian skeleton as obtained for the stationary cat eyes. The hyperbolic fixed point at the origin and its stable and unstable manifolds are clearly visible. Also elliptic fixed points at positions $(-\pi, 0)$ and $(\pi, 0)$ are visible. Figure b) shows a set of initial scalar fields and c) shows the evolution of the three patches: the one in cyan shows filamentation, the other staying coherent (in blue) and the third done showing a tongue formation (in red) similar to the one observed for the Potential Vorticity in Figure 4. Colors are chosen to highlight the analogous features visible in Figure 4. Clearly Figures 5 b) and c) show time dependent patterns, however the Lagrangian skeleton shown in a) is stationary.

4.1 ~~3D Lagrangian structures over Antarctica~~

5 3D Lagrangian structures over Antarctica

The strong and cyclonic SPV characteristic of the winter circulation above Antarctica ~~is typically represented~~ has been typically represented in the literature by cross sections such as those in Figs. 2 and 4. In this section we ~~attempt to improve on~~ will improve this representation with figures that are more revealing of the full 3D description of the circulation. Figure 6 shows for a day in late winter 1979 (15th of August) the representation of M obtained for $\tau = 5$ for the vertical slice passing through

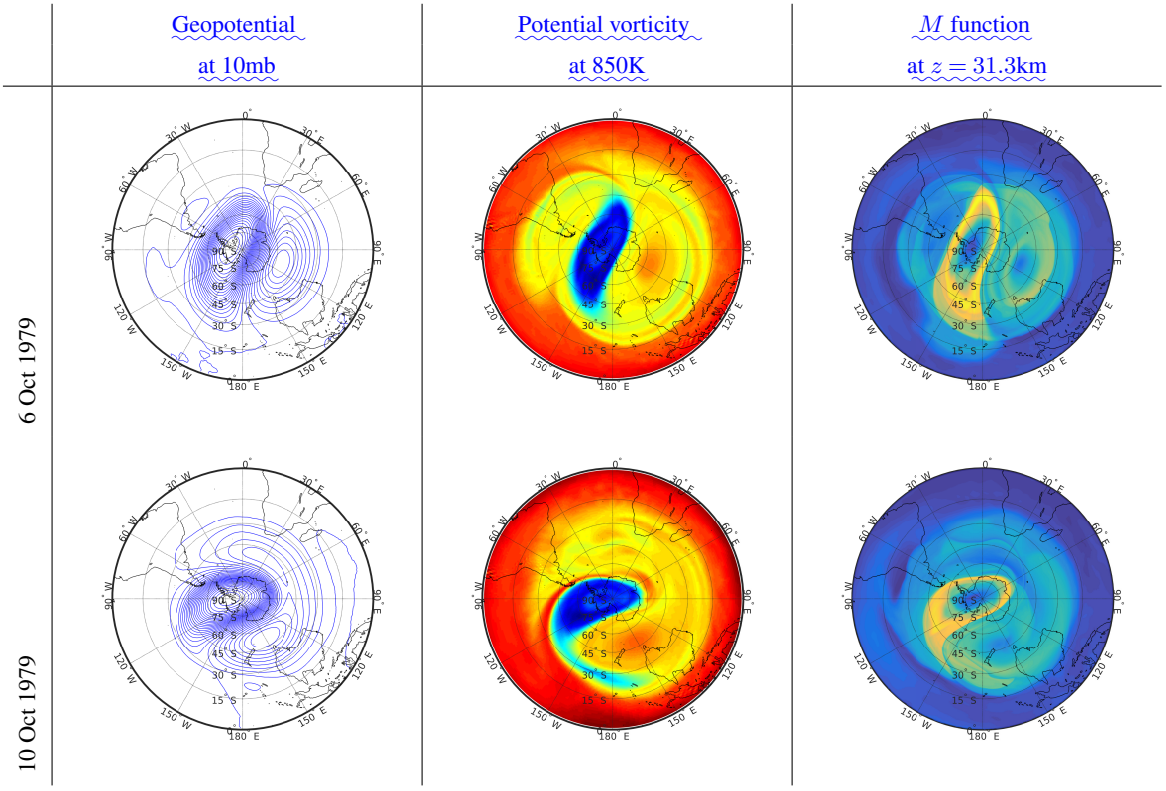

Figure 4. Comparison of Geopotential at constant Pressure 10mb, Potential Vorticity at 850K and M function at $z = 31.3$km for several days of October 1979

longitudes 90^{o}W and 90^{o}E. An outstanding feature in this representation is the bright yellow color highlighting a coherent structure. This feature captures the SPV as a tubular structure, similar to those described in Figure 1b), with walls around 60^{0}S and an approximately vertical axis coinciding with that of the Earth and extending from the uppermost level of data down to between 15 and 20 km height, i.e. the transition between the troposphere and stratosphere (tropopause). ~~On the one hand, the~~ In this case however the average of M does not converge as the flow is aperiodic (see Lopesino *et al.* (2017)), and thus contours of M are not strictly representing invariant sets. Despite this, the setting is analogous to that described for the vortices in the example of section 2. Additionally, the greenish colors that extend equatorward between 15 and 20 km, both at the west and the east, capture the upper tropospheric subtropical westerly jets. Specifically at the west , the greenish colors extend downwards up to the equator (90^{o}W) suggesting that the structures involve the entire atmospheric layer. We can also clearly see evidence of the very different dynamical character of the troposphere and stratosphere. Whilst the former region is practically dominated by the SPV, the latter shows much more fine detail reflected by an intricate line pattern. This tangled pattern is the manifestation of crossings of stable and unstable manifolds, which are associated with strong and fast mixing processes at the lowest atmospheric levels. This image is consistent and complementary to the projection at 10 km presented in Figure 2c) and d) and also to the one described next.

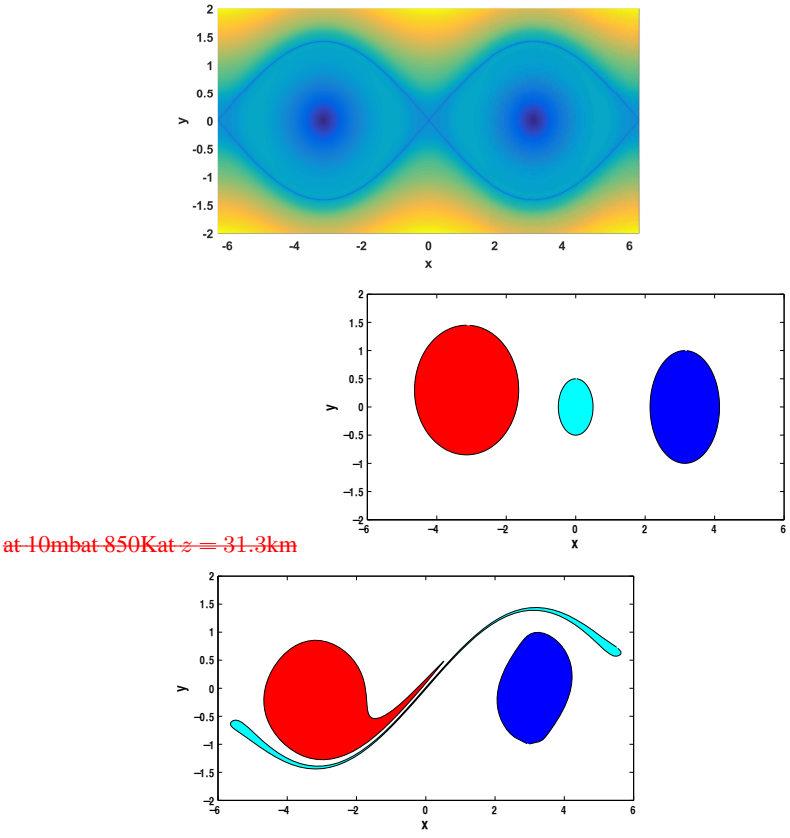

Figure 5. ~~Comparison of Geopotential at constant Pressure 10mb, Potential Vorticity at 850K and M function at $z = 31.3$km~~ a) Lagrangian skeleton for ~~several days~~ the stationary cat eyes; b) three initial patches of ~~October 1979~~a purely advective field; c) evolution of the patches at time $t = 5.6$

The description of the vortex on the 15th August 1979 is supplemented by Fig. 7, which shows the function M computed for ~~$\tau = 5$~~ $\tau = 10$ along a vertical slice through latitude 60°S, where most of the SPV walls are. The intricate structures in the troposphere are also apparent in this figure. In addition, a wavy structure is clearly visible at the boundary between troposphere and stratosphere. In terms of a Fourier decomposition of M at constant height in Fig. 7, we can see the classical pattern of longer wavelengths dominating the field as height increases. At tropopause level, a wavenumber 4 component is clearly visible while at the upper part of the vortex a wavenumber 2 is evident (Manney *et al.*, 1991). The vertical propagation of these features across the stratosphere from the 8th to the 21st of August of 1979 is clearly visible in the attached movie S1.

We next focus on the description of the 3D Lagrangian structures for the period 6-18 October 1979. Figure 8 shows the rapid changes of the SPV that took place in October 1979 as the lower polar stratosphere warmed up strongly during the spring season (Yamazaki and Mechoso, 1985). The figure shows the function M computed for $\tau = 5$ along a vertical slice passing through latitude 60°S for several October dates. Subplots a), b), c) and d) in Figure 8 confirm that Lagrangian structures in the

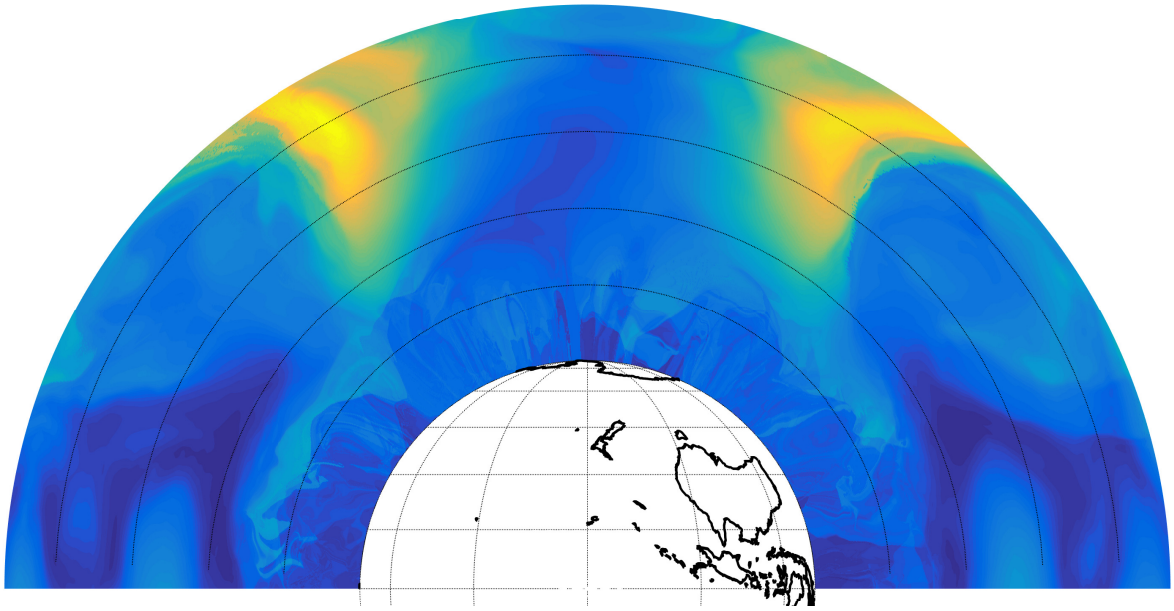

Figure 6. 15 August 1979 00:00:00 UTC. M for $\tau = 5$ days displayed along the vertical slice passing through longitudes 90^oW and 90^oE. The black lines on the stratosphere correspond to ~~height~~ heights 10, 20, 30 and 40km and black lines on the Earth's surface correspond to latitudes $15^o, 30^o, 45^o, 60^o, 75^o$ south.

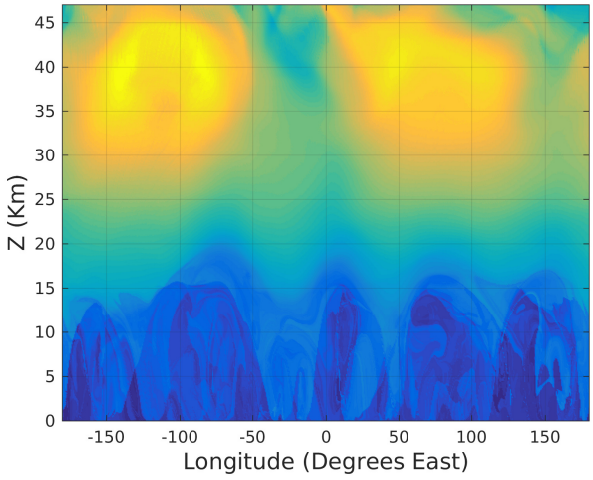

Figure 7. 15 August 1979 00:00:00 UTC. M for $\tau = 5$ days displayed along the vertical slice passing through latitude 60°S.

stratosphere become more complex in the warming period. On the 18th of October no yellow coherent features are visible in the upper stratosphere.

To help in the interpretation of Fig. 8, Fig. 9 displays horizontal sections of M on the 6th of October at different heights $z = 10$km, 21.2km, 31.3km and 40km ~~. Figure 8 shows sharp contrasts~~ as well as a vertical section along meridians 90^oE, 90^oW. Figures 8 and 9 show important differences with the winter conditions two months earlier visible in Figs. 6 and 7. The ~~structure representing the cyclonic vortex tube flow is now approximately centered off the pole above the Antarctic Peninsula at lower levels in the stratosphere. The~~ 60°S section in Fig. 8 a) intersects the cyclonic vortex four times mostly in the western hemisphere. Another deep, anticyclonic vortex appears in the eastern hemisphere above 25km. ~~This is~~ These cyclonic and anticyclonic vortices are also evident in Fig. ~~8 a), Fig.~~ 9a) at $z = 31.3$km and $z = 40$km, and in Fig. 9b). ~~Mechoso and Hartmann (1982) suggest that the preferred geographical location (ridge south of Australia) for development of the anticyclonic vortex indicate that the stratospheric circulation is governed to a significant extent from below. This anticyclonic vortex will strengthen and eventually dominate at high levels. In terms of Fourier components, a quasi-stationary wave 1 amplifies on this date, in conjunction with the displacement of the cyclonic vortex from the polar position. These subplots confirm the intricate Lagrangian structures in the troposphere. The 18th of October no yellow coherent features are visible in the upper stratosphere. The lowest of the horizontal sections, taken within the troposphere, confirms its chaotic nature.~~

~~a) 6 October 1979 b) 10 October 1979c) 14 October 1979 d) 18 October 1979Vertical slices showing M for $\tau = 5$ at constant latitude 60°S at four selected days in October. The color scale is the same in all figures.~~

~~a)$z = 10$km $z = 21.2$km~~ In particular in the projection of Fig. 9a) at $z = 31.3$~~km $z = 40$kmb)6 October 1979 00:00:00 UTC. a) Slices of M at constant heights $z = 10, 21.2, 31.3$ and 40km with $\tau = 5$; b) Slice of M at constant longitude $\lambda = 90°W$ and $\lambda = 90°E$). The black lines in b) correspond to 10, 20, 30 and 40km.~~ km, along the longitude 0^o, between latitudes 30^o-45^o south, crossing lines marked with a white arrow show the presence of a hyperbolic point, being its unstable manifold the separatrix between the two vortices. The vertical extension of this hyperbolic trajectory is depicted with the red line in Figure 9c). This figure shows the analogue to the normally hyperbolic invariant curve explained in Section 2 with the additional feature that here the flow is time dependent, while, for simplicity, the example in Section 2 was stationary. Figure 1b) sketches the correspondant typical configuration for two counter-rotating vortex tubes illustrating this description.

~~We next address how~~ The vertically extended unstable manifold of the normally hyperbolic invariant curve that separates the two vortex tubes is captured by M ~~captures the invariant character of singular features found in the representations of M.~~ and is visible in Figure 8 a) ~~shows a blue dark line~~ and Fig. 9b) as a narrow dark blue line in an analogous way to that presented in Figure 1. The first of these two figures shows it near the edge of the polar vortex, around 45°E ~~. This feature is related to an invariant manifold that~~ marked with a white arrow, and for the latter also a white arrow points to the described feature. This manifold structure is separating the two counterrotating vortex tubes just described. It acts as a vertical barrier, which is several kilometers deep ~~. This manifold structure is separating the two counterrotating vortex tubes just described~~as is the case for the unstable manifolds associated to a normally hyperbolic invariant curve formed of hyperbolic trajectories at each h level. Further information on the singular features is given in Fig. 10. The black dots in Figs. 10a) and b) represents for the 6th of

October 1979, 00:00:00 UTC, the horizontal and vertical positions of a particle located on the feature indicated by the blue dark line ~~in Fig. 8 a)~~ at a height of 31.3km, longitude 90°E and latitude 77.74°S. The black dots in Figs. 10c) and d) show the corresponding locations of the same particle six hours later. The invariant character of the singular structure is confirmed as the particle remains on it during its evolution~~.~~

~~Similarly, let us consider a particle located at~~ , and its unstable character is confirmed by the fact that the particle moves away from the hyperbolic point~~appearing in Fig. 9 a) at $z = 31.3$km at around 12°E. Figure **??** shows the~~ .

Mechoso and Hartmann (1982) have suggested that the fact that the preferred geographical location (ridge south of Australia) for the development of this anticyclonic vortex in this particular event indicates that the stratospheric circulation is governed to a significant extent from below (see also Quintanar and Mechoso (1995)). This anticyclonic vortex will strengthen and eventually dominate at high levels. In terms of Fourier components, a quasi-stationary wave 1 amplifies on this date, in conjunction with the displacement of the cyclonic vortex from the polar position.

~~a)6 of October 1979 00:00:00 UTC b) 6 of October 1979 12:00:00 UTC.c) 6 of October 1979 18:00:00 UTC d) 7 of October 1979 12:00:00 UTC.e)7 of October 1979 18:00:00 UTC f)8 of October 1979 00:00:00 UTC.Evaluation of the M function with a black particle at different longitudes. a) The black particle is placed on an invariant manifold on a 2D slice obtained at constant longitude 12^{o}W on the 6 of October 1979 00:00:00 UTC; b) the same black particle on a plane with constant longitude on the 6 of October 1979 12:00:00 UTC; c) the black particle on a plane with constant longitude on the 6 of October 1979 18:00:00 UTC; d) the black particle on a plane with constant longitude on the 7 of October 1979 12:00:00 UTC; e) the black particle on a plane with constant longitude on the 7 of October 1979 18:00:00 UTC; f) the black particle on a plane with constant longitude on the 8 of October 1979 00:00:00 UTC.~~

6 Conclusions

In the present paper we ~~have introduced an algorithm for the visualization , analysis and validation of transport and mixing processes in~~ discuss the visualization of three-dimensional Lagrangian structures in atmospheric flows. ~~The algorithm~~ Specifically, we have explained mathematical aspects about the Lagrangian geometrical structures to be expected in the atmospheric setting in 3D and have introduced the concept of normally hyperbolic invariant curves in an specific example which recover features of those observed in the stratosphere. The algorithm used to represent the 3D Lagrangian structures is based on the methodology of Lagrangian descriptors (LDs)~~, a technique from Dynamical Systems Theory. Specifically, we have implemented~~ . We have explored the application of the full power of the function M computed with 3D trajectories, which hitherto had been used in 2D settings. The consistency of our development ~~was verified by showing the similarity of results obtained from the full~~ has been verified by comparing the 3D scenario results at a constant height with those obtained from the 2D scenario ~~for a potential temperature surface that is at approximately the same height~~in potential temperature surfaces at equivalent heights.

To demonstrate the methodology we have applied it to a numerical dataset describing the flow above Antarctica during the southern ~~late~~ mid-late winter and spring~~, with an emphasis on the final stratospheric warming of 1979.~~ . The dataset was obtained from ERA-Interim Reanalysis data provided by the ECMWF. Our findings show the vertical extension and structure of

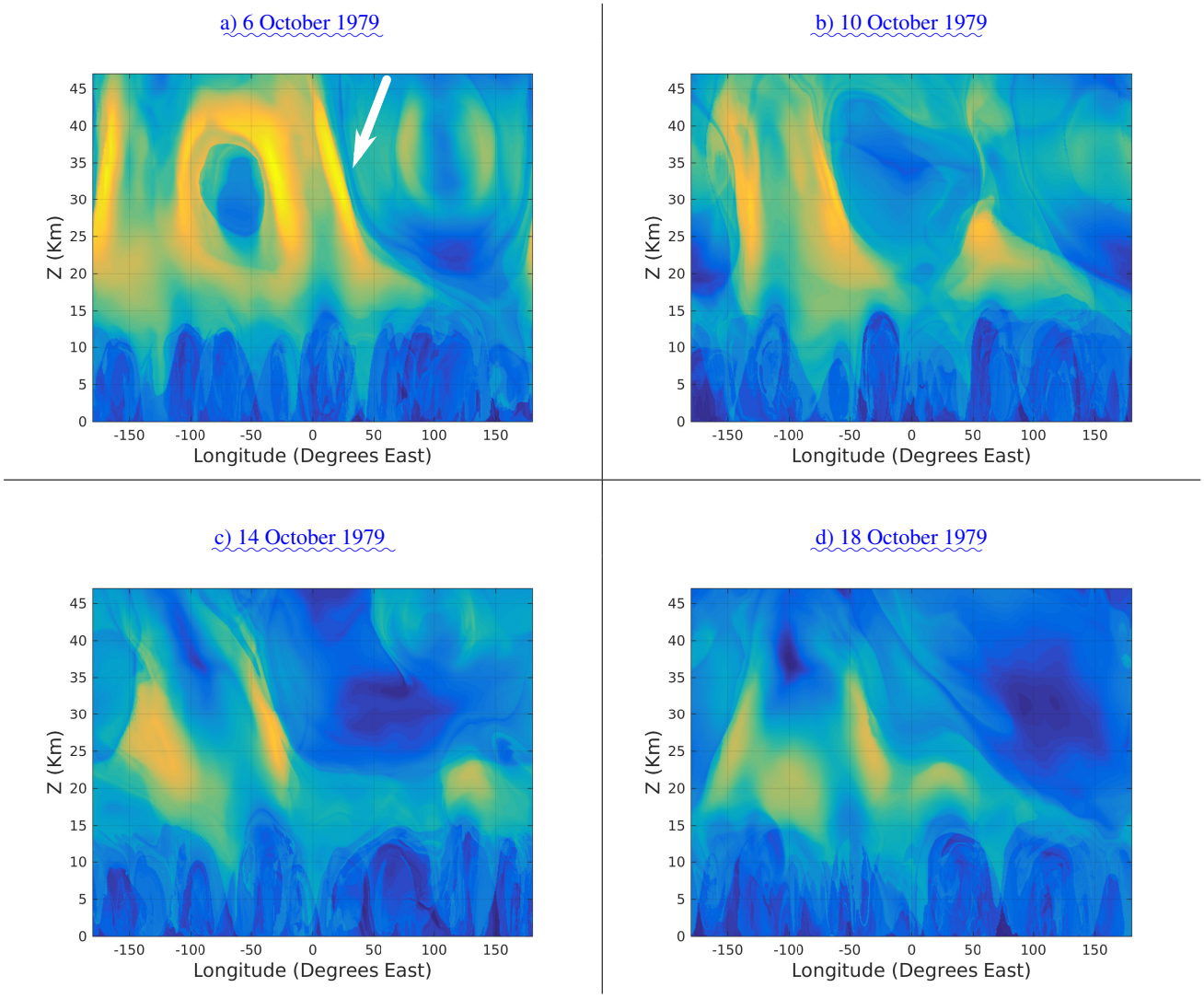

Figure 8. Vertical slices showing M ~~function for a sequence of 2D slices obtained each at constant longitude. From one panel to the next, longitude changes tracking the particle motion. Again the invariant nature of~~ for $\tau = 5$ at constant latitude 60°S at four selected days in October. The color scale is the ~~singular structures is confirmed while the particle evolves. Between frames a~~ same in all figures.

the stratospheric polar vortex and its evolution. We also characterize, from the Lagrangian point of view, the boundary between the troposhere and the stratosphere. Very complex Lagrangian patterns are identified in the troposphere, which support the presence of strong mixing processes. The "final stratospheric warming" is characterized by the breakdown of the westerly SPV during the transition from winter to summer circulation. Our results confirm that the onset of this process is characterized by an initial decay of the vortex in the upper stratosphere where the circulation weakens, albeit it remains strong at lower heights. We have also captured the anticyclonic circulation that develops during October preferentially above the southern part of Australia.

~~A preliminary analysis of the 3D features provided by the methodology has provided insights that will be explored in future studies. The cyclonic westerly vortex during late winter appears to extend down to the troposphere. We have also found features related to invariant manifolds that can act as a vertical barriers to transport between vortices~~We illustrate the vertical structure of these two counterrotating vortices, and the invariant separatrix that divides them. The particular feature found is several kilometers deep and we demonstrated that fluid parcels remain in this feature during intervals in the order of days. Such features ~~may be important for~~ highlight the complexities in the transport of chemical tracers in the stratosphere.

Acknowledgements. J. Curbelo, V. J. García-Garrido and A. M. Mancho are supported by MINECO grant MTM2014-56392-R. C. Niang acknowledges Fundacion Mujeres por Africa and ICMAT Severo Ochoa project SEV-2011-0087 for financial support. A. M. Mancho and C. Niang are supported by CSIC grant COOPB20265. The research of S. Wiggins is supported by ONR grant No. N00014-01-1-0769. C. R. Mechoso was supported by the U.S. NSF grant AGS-1245069. We also acknowledge support from ONR grant No. N00014-16-1-2492.

References

Aref, H. (1984). Stirring by chaotic advection. *J. Fluid Mech.*, **143**, 1–21.

Aurell, E., Boffeta, G., Crisanti, A., Paladin, G., and Vulpiani, A. (1997). Predictability in the large: An extension of the concept of Lyapunov exponent. *J. Phys. A :Math. Gen.*, **30**, 1–26.

Bettencourt, J. H., López, C., Hernández-García, E., Montes, I., Sudre, J., Dewitte, B., Paulmier, A., and Garçon, V. (2014). Boundaries of the peruvian oxygen minimum zone shaped by coherent mesoscale dynamics. *Nature Geoscience*, **8**, 937–940.

Bower, A. S. (1991). A simple kinematic mechanism for mixing fluid parcels across a menadering jet. *J. Phys. Oceanogr.*, **21**, 173–180.

Bowman, K. P. (1993). Large-scale isentropic mixing properties of the Antarctic polar vortex from analyzed winds. *Journal of Geophysical Research*, **98**, 23013–23027.

Bowman, K. P. (2006). Transport of carbon monoxide from the tropics to the extratropics. *Journal of Geophysical Research: Atmospheres*, **111**(D2).

Branicki, M. and Kirwan Jr., A. D. (2010). Stirring: The Eckart paradigm revisited. *Int. J. Eng. Sci.*, **48**, 1027–1042.

Branicki, M. and Wiggins, S. (2009). An adaptive method for computing invariant manifolds in non-autonomous, three-dimensional dynamical systems. *Physica D*, **238**(16), 1625 – 1657.

Branicki, M., Mancho, A. M., and Wiggins, S. (2011). A Lagrangian description of transport associated with a front-eddy interaction: application to data from the North-Western Mediterranean sea. *Physica D*, **240**(3), 282–304.

Cartwright, J. H. E., Feingold, M., and Piro, O. (1996). Chaotic adection in three-dimensional unsteady incompressible laminar flow. *J. Fluid Mech.*, **316**, 259–284.

Charlton, A. J., O'Neill, A., Lahoz, W. A., and Berrisford, P. (2006). The splitting of the stratospheric polar vortex in the southern hemisphere, september 2002: Dynamical evolution. *J. Atmos. Sci.*, **66**, 590–602.

de la Cámara, A., Mancho, A. M., Ide, K., Serrano, E., and Mechoso, C. (2012). Routes of transport across the Antarctic polar vortex in the southern spring. *J. Atmos. Sci.*, **69**(2), 753–767.

de la Cámara, A., Mechoso, R., Mancho, A. M., Serrano, E., and Ide., K. (2013). Isentropic transport within the Antarctic polar night vortex: Rossby wave breaking evidence and Lagrangian structures. *J. Atmos. Sci.*, **70**, 2982–3001.

Dee, D. P. *et al.* (2011). The ERA-Interim reanalysis: configuration and performance of the data assimilation system. *Quarterly Journal of the Royal Meteorological Society*, **137**(656), 553–597.

d'Ovidio, F., Isern-Fontanet, J., López, C., Hernández-García, E., and García-Ladona, E. (2009). Comparison between Eulerian diagnostics and finite-size Lyapunov exponents computed from altimetry in the Algerian basin. *Deep Sea Res. I*, **56**(1), 15–31.

Dritschel, D. G. (1989). Contour dynamics and contour surgery: numerical algorithms for extended, high-resolution modelling of vortex dynamics in two-dimensional, inviscid, incompressible flows. *Comput. Phys. Rep.*, **10**, 77–146.

du Toit, P. C. and Marsden, J. E. (2010). Horseshoes in hurricanes. *J. Fixed Point Theory Appl.*, **7**, 351–384.

Farazmand, M. and Haller, G. (2012). Computing Lagrangian Coherent Structures from variational LCS theory. *Chaos*, **22**, 013128.

Garcia-Garrido, V. J., Mancho, A. M., and Wiggins, S. (2015). A dynamical systems approach to the surface search for debris associated with the disappearance of flight MH370. *Nonlin. Proc. Geophys.*, **22**, 701–712.

Garcia-Garrido, V. J., Ramos, A., Mancho, A. M., Coca, J., and Wiggins, S. (2016). A dynamical systems perspective for a real-time response to a marine oil spill. *Marine Pollution Bulletin.*, pages 1–10.

García-Garrido, V. J., Curbelo, J., Mechoso, C. R., Mancho, A. M., and Wiggins, S. (2017). A simple kinematic model for the lagrangian description of relevant nonlinear processes in the stratospheric polar vortex. *Nonlin. Proc. Geophys. Discussion*.

Guha, A., Mechoso, C. R., Konor, C. S., and Heikes, R. P. (2016). Modeling rossby wave breaking in the southern spring stratosphere. *J. Atmos. Sci.*, **73**(1), 393–406.

Haller, G. (2000). Finding finite-time invariant manifolds in two-dimensional velocity fields. *Chaos*, **10**(1), 99–108.

Haller, G. (2001). Distinguished material surfaces and coherent structures in three-dimensional fluid flows. *Physica D*, **149**, 248–277.

Haller, G. and Beron-Vera, F. J. (2012). Geodesic theory of transport barriers in two-dimensional flows. *Physica D*, **241**(7), 1680–1702.

Haller, G. and Yuan, G. (2000). Lagrangian coherent structures and mixing in two-dimensional turbulence. *Physica D*, **147**, 352–370.

Holton, J. R. (2004). *An Introduction to Dynamic Meteorology*. Elsevier Academic Press.

Ide, K., Small, D., and Wiggins, S. (2002). Distinguished hyperbolic trajectories in time dependent fluid flows: analytical and computational approach for velocity fields defined as data sets. *Nonlin. Proc. Geophys.*, **9**, 237–263.

Joseph, B. and Legras, B. (2002). Relation between kinematic boundaries, stirring, and barriers for the Antarctic polar vortex. *J. Atmos. Sci.*, **59**, 1198–1212.

Ju, N., Small, D., and Wiggins, S. (2003). Existence and computation of hyperbolic trajectories of aperiodically time-dependent vector fields and their approximations. *Int. J. Bif. Chaos*, **13**, 1449 –1457.

Juckes, M. N. and McIntyre, M. E. (1987). A high-resolution one-layer model of breaking planetary waves in the stratosphere. *Nature*, **328**, 590–596.

Krüger, K., Naujokat, B., and Labitzke, K. (2005). The unusual midwinter warming in the southern hemisphere stratosphere 2002: A comparison to northern hemisphere phenomena. *J. Atmos. Sci.*, **62**, 603–613.

Lekien, F. and Ross, S. D. (2010). The computation of finite-time lyapunov exponents on unstructured meshes and for non-euclidean manifolds. *Chaos*, **20**, 017505.

Lopesino, C., Balibrea-Iniesta, F., Wiggins, S., and Mancho, A. M. (2015). Lagrangian descriptors for two dimensional, area preserving autonomous and nonautonomous maps. *Communications in Nonlinear Science and Numerical Simulations*, **27**(1-3), 40–51.

Lopesino, C., Balibrea-Iniesta, F., García-Garrido, V. J., Wiggins, S., and Mancho, A. M. (2017). A theoretical framework for lagrangian descriptors. to appear. *International Journal of Bifurcation and Chaos.*

Madrid, J. A. J. and Mancho, A. M. (2009). Distinguished trajectories in time dependent vector fields. *Chaos*, **19**, 013111.

Malhotra, N. and Wiggins, S. (1998). Geometric structures, lobe dynamics, and Lagrangian transport in flows with aperiodic time-dependence, with applications to Rossby wave flow. *J. Nonlinear Science*, **8**, 401–456.

Mancho, A. M., Small, D., Wiggins, S., and Ide, K. (2003). Computation of Stable and Unstable Manifolds of Hyperbolic Trajectories in Two-Dimensional, Aperiodically Time-Dependent Vectors Fields. *Physica D*, **182**, 188–222.

Mancho, A. M., Small, D., and Wiggins, S. (2004). Computation of hyperbolic trajectories and their stable and unstable manifolds for oceanographic flows represented as data sets. *Nonlin. Proc. Geophys.*, **11**, 17–33.

Mancho, A. M., Small, D., and Wiggins, S. (2006a). A comparison of methods for interpolating chaotic flows from discrete velocity data. *Computers and Fluids*, **35**, 416–428.

Mancho, A. M., Hernández-García, E., Small, D., Wiggins, S., and Fernández, V. (2006b). Lagrangian transport through an ocean front in the North-Western Mediterranean Sea. *J. Phys. Oceanogr.*, **38**(6), 1222–1237.

Mancho, A. M., Small, D., and Wiggins, S. (2006c). A tutorial on dynamical systems concepts applied to Lagrangian transport in oceanic flows defined as finite time data sets: Theoretical and computational issues. *Phys. Rep.*, **237**(3-4), 55–124.

Mancho, A. M., Wiggins, S., Curbelo, J., and Mendoza, C. (2013). Lagrangian descriptors: A method for revealing phase space structures of general time dependent dynamical systems. *Communications in Nonlinear Science and Numerical Simulations*, **18**(12), 3530–3557.

Manney, G. L. and Lawrence, Z. D. (2016). The major stratospheric final warming in 2016: Dispersal of vortex air and termination of Arctic chemical ozone loss. *Atmospheric Chemistry and Physics Discussions*, **2016**, 1–40.

Manney, G. L., Farrara, J. D., and Mechoso, C. R. (1991). The behavior of wave 2 in the southern hemisphere stratosphere during late winter and early spring. *J. Atmos. Sci.*, **48**, 976–998.

Manney, G. L., Sabutis, J. L., Alley, D. R., Lahoz, W. A., Scaife, A. A., Randall, C. E., Pawson, S., Naujokat, B., and Swinbank, R. (2006). Simulations of dynamics and transport during the september 2002 antarctic major warming. *J. Atmos. Sci.*, **66**(690-707).

McIntyre, M. E. and Palmer, T. N. (1983). Breaking planetary waves in the stratosphere. *Nature*, **305**, 593–600.

McIntyre, M. E. and Palmer, T. N. (1984). The surf zone in the stratosphere. *Journal of Atmospheric and Terrestrial Physics*, **46**(9), 825–849.

McIntyre, M. E. and Palmer, T. N. (1985). A note on the general concept of wave breaking for rossby and gravity waves. *Pure and Applied Geophysics*, **123**(6), 964–975.

Mechoso, C. R. and Hartmann, D. L. (1982). An observational study of traveling planetary waves in the southern hemisphere. *Journal of the Atmospheric Sciences*, **39**(9), 1921–1935.

Mechoso, C. R., O'Neill, A., Pope, V. D., and Farrara, J. D. (1988a). A study of the stratospheric final warming of 1982 in the southern hemisphere. *Quarterly Journal of the Royal Meteorological Society*, **114**(484), 1365–1384.

Mechoso, C. R., O'Neill, A., Pope, V. D., and Farrara, J. D. (1988b). A study of the stratospheric final warming of 1982 in the Southern Hemisphere. *Quart. J. R. Meteor. Soc.*, **114**, 1365–1384.

Mendoza, C. and Mancho, A. M. (2010). The hidden geometry of ocean flows. *Phys. Rev. Lett.*, **105**(3), 038501.

Mendoza, C. and Mancho, A. M. (2012). The Lagrangian description of aperiodic flows: a case study of the Kuroshio Current. *Nonlin. Proc. Geophys.*, **19**(14), 449–472.

Mendoza, C., Mancho, A. M., and Wiggins, S. (2014). Lagrangian descriptors and the assesment of the predictive capacity of oceanic data sets. *Nonlin. Proc. Geophys.*, **21**, 677–689.

Mezić, I. and Wiggins, S. (1994). On the integrability and perturbation of three-dimensional fluid flows with symmetry. *Journal of Nonlinear Science*, **4**(1), 157–194.

Mezic, I. and Wiggins, S. (1999). A method for visualization of invariant sets of dynamical systems based on the ergodic partition. *Chaos*, **9**(1), 213–218.

Moharana, N. R., Speetjens, M. F. M., Trieling, R. R., and Clercx, H. J. H. (2013). Three-dimensional lagrangian transport phenomena in unsteady laminar flows driven by a rotating sphere. *Phys. Fluids*, **25**, 093602.

Morales-Juberías, R., Sayanagi, K. M., Simon, A. A., Fletcher, L. N., and Cosentino, R. G. (2015). Meandering shallow atmospheric jet as a model of saturn's north-polar hexagon. *The Astrophysical Journal Letters*, **806**, L18 (6pp).

Nakamura, M. and Plumb, R. A. (1994). The effects of flow asymmetry on the direction of rossby wave breaking. *J. Atmos. Sci.*, **51**, 2031–2044.

Ottino, J. M. (1989). *The Kinematics of Mixing: Stretching, Chaos, and Transport*. Cambridge University Press, Cambridge, England. Reprinted 2004.

Polvani, L. M. and Plumb, R. A. (1992). Rossby wave breaking, microbreaking, filamentation, and secondary vortex formation: The dynamics of a perturbed vortex. *J. Atmos. Sci.*, **49**(6), 462–476.

Pouransari, Z., Speetjens, M. F. M., and Clercx, H. J. H. (2010). Formation of coherent structures by fluid inertia in three-dimensional laminar flows. *J. Fluid Mech.*, **654**, 5–34.

Press, W. H., Teukolsky, S. A., Vetterling, W. T., and Flannery, B. P. (1992). *Numerical Recipes in C: The Art of Scientific Computing*. Cambridge University Press, New York, NY, USA.

Quintanar, A. I. and Mechoso, C. R. (1995). Quasi-stationary waves in the southern hemisphere. part i: Observational data. *J. Climate*, **4**, 2659–2672.

Rabier, F. *et al.* (2010). The concordiasi project in antarctica. *Bulletin of the American Meteorological Society*, **91**(1), 69–86.

Rempel, E. L., Chian, A. C.-L., Brandenburg, A., Munuz, P. R., and Shadden, S. C. (2013). Coherent structures and the saturation of a nonlinear dynamo. *Journal of Fluid Mechanics*, **729**, 309–329.

Rutherford, B. and Dangelmayr, G. (2010). A three-dimensional lagrangain hurricane eyewall computation. *Quarterly Journal of the Royal Meteorological Society*, **136**, 1931–1944.

Rutherford, B., Dangelmayr, G., and Montgomery, M. T. (2012). Lagrangian coherent structures in tropical cyclone intensification. *Atmospheric Chemistry and Physics*, **12**, 5483–5507.

Rypina, I. I., Brown, M. G., Beron-Vera, F. J., Kocak, H., Olascoaga, M. J., and Udovydchenkov, I. A. (2007). On the lagrangian dynamics of atmospheric zonal jets and the permeability of the stratospheric polar vortex. *J. Atmos. Sci.*, **64**, 3595–3610.

Rypina, I. I., Pratt, L. J., Wang, P., Özgökmen, T. M., and Mezic, I. (2015). Resonanace phenomena in a time-dependent, three-dimensional model of an idealized eddy. *Chaos*, **25**, 087401.

Samelson, R. and Wiggins, S. (2006). *Lagrangian Transport in Geophysical Jets and Waves: The Dynamical Systems Approach*. Springer-Verlag, New York.

Samelson, R. M. (1992). Fluid exchange across a meandering jet. *J. Phys. Oceanogr.*, **22**(4), 431–440.

Shadden, S. C., Lekien, F., and Marsden, J. E. (2005). Definition and properties of Lagrangian Coherent Structures from finite-time Lyapunov exponents in two-dimensional aperiodic flows. *Physica D*, **212**, 271–304.

Simmons, A., Uppala, S., Dee, D., and S, K. (2007). ERA-Interim: New ECMWF reanalysis products from 1989 onwards. *ECMWF Newsletter*, **110**, 25–35.

Smith, M. L. and McDonald, A. J. (2014). A quantitative measure of polar vortex strength using the function m. *J. Gephys.Res. Atmos.*, **119**, 5966–5985.

Snyder, J. P. (1987). *Map Projections–A Working Manual*. U.S. Geological Survey professional paper. U.S. Government Printing Office.

Stewartson, K. (1977). The evolution of the critical layer of a rossby wave. *Geophysical & Astrophysical Fluid Dynamics*, **9**(1), 185–200.

Warn, T. and Warn, H. (1978). The evolution of a nonlinear critical level. *Studies in Applied Mathematics*, **59**(1), 37–71.

Wiggins, S. (1988). *Global bifurcations and chaos: analytical methods*, volume 73. Springer Verlag.

Wiggins, S. (2010). Coherent structures and chaotic advection in three dimensions. *J. Fluid Mech.*, **654**, 1–4.

Yamazaki, K. and Mechoso, C. R. (1985). Observations of the final warming in the stratosphere of the southern hemisphere during 1979. *J. Atmos. Sci.*, **42**, 1198–1205.

c)to c) the particle approaches a hyperbolic point along the stable manifold, which is visible in the different slices. From frame d) onwards the particle r

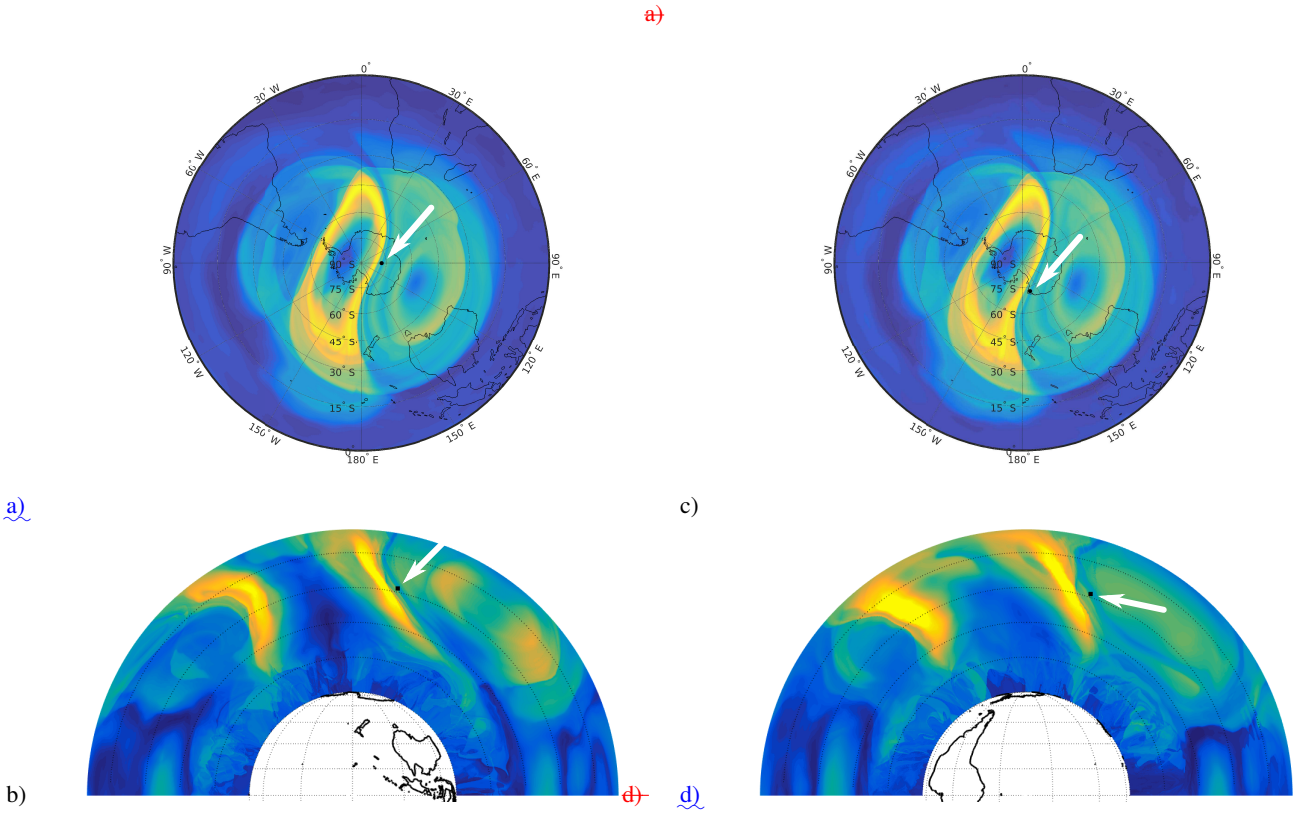

Figure 10. Evaluation of the M function with a black particle on it. a) The black particle is placed exactly over an invariant manifold on a 2D slice obtained at height of 31.3 km on the 6 of October 1979 00:00:00 UTC; b) the same black particle on the same day and time placed on a 2D slice obtained at longitude $90^o E$; c) the same black particle six hours later on a 2D slice of M obtained at the corresponding height of the particle at that time; d) the same black particle six hours later on a 2D slice of M obtained at the corresponding longitude of the particle at that time.